SAND2021-7226C

Properties of PV Cell Fractures and Effects on Performance of Al-BSF and PERC Modules

Carolina M. Whitaker*, Benjamin G. Pierce*, Roger H. French*, Jennifer L. Braid*†
*SDLE Research Center, Materials Science Department, Case Western Reserve University, Cleveland, OH, 44106, USA
†Sandia National Laboratories, Albuquerque, NM, 87123, USA

***Abstract*—Cell cracking in PV modules can lead to a variety of changes in module operation, with vastly different performance degradation based on the type and severity of crack. In this work, we demonstrate automated measurement of cell crack properties from electroluminescence images, and correlate these properties with current-voltage curve features on 35 four-cell Al-BSF and PERC mini-modules showing a range of crack types and severity. Impacts of cracking on electrical performance demonstrated in this work include cell shunting, electrical isolation of cell regions, and increased series resistance, with Al-BSF and PERC cells showing different crack-related power loss mechanisms.**

***Index Terms*—PV module, electroluminescence, cell cracks, shunting, computer vision**

I. Introduction

Throughout a PV module's lifetime, it is exposed to several mechanical stresses, making the delicate silicon cells susceptible to cracking. Causes of cell cracking may include transportation, handling, installation, severe weather, and other events [1]–[5]. Microcracks in the silicon initiated during manufacturing may also develop into larger cracks during the module's lifetime due to weather-related loads and thermal conditions [6]–[10]. Severe cell cracking has been known to reduce the power output of PV modules, with the impact on electrical performance worsening over time [8], [11]–[14]. To diagnose cracks in PV modules, photoluminescence (PL) [15] and electroluminescence (EL) [16] imaging are frequently used. Both imaging techniques can identify cell irregularities and fractures within modules that are not visible to the naked eye. Cracks have been described by their orientation: diagonal, perpendicular, or parallel to the cell busbars; and as branching (dendritic) or linear [17], [18]. In this paper, we examine several types of cracks in PV modules and characterize them based on their physical properties via digital image processing methods applied to EL images. We also study how geometric properties of the cracks align with the electrical characteristics of the modules, and statistically compare the distributions of crack and electrical performance features for Aluminum Back Surface Field (Al-BSF) and Passivated Emitter and Rear Contact (PERC) cells and mini-modules. This study demonstrates a framework to diagnose and characterize cell cracks in PV modules in an automated fashion, as well as link fracture characteristics to mechanistic changes in module performance.

This material is based upon work supported by the U.S. Department of Energy's Office of Energy Efficiency and Renewable Energy (EERE) under Solar Energy Technologies Office (SETO) Agreement Number DE-EE-0008550. The views expressed herein do not necessarily represent the views of the U.S. Department of Energy or the United States Government. Sandia National Laboratories is a multimission laboratory managed and operated by National Technology & Engineering Solutions of Sandia, LLC, a wholly owned subsidiary of Honeywell International Inc., for the U.S. Department of Energy's National Nuclear Security Administration under contract DE-NA0003525.

II. Experimental Methods

A. Sample Set

In this sample set, there are 35 four-cell mini-modules; 19 fabricated with Al-BSF cells, and 16 with PERC cells. Al-BSF and PERC cells mainly differ in their back contact layer: Al-BSF cells have a full surface back layer made of screen printed aluminum paste, while PERC cells have an added dielectric passivation layer that enables local contacts between the silicon and the rear aluminum surface. This added dielectric layer in the PERC cells increases light capture and reduces rear-side recombination, improving overall cell efficiency. All cells in this study were made with monocrystalline Longi p-type silicon and had LDEC-style n-type diffusion and four busbars. Each mini-module is tabbed between cells to a central junction box, allowing for individual measurements of each cell, and measurement of all four cells in series. Due to improper shipping from California to Cleveland, OH, all modules in this sample set experienced mild to severe cell cracking.

B. Measurements

This project studies the effects of cell cracks on electrical performance at both the mini-module and single cell levels. Cell and mini-module measurements include I-V curves, and EL and PL images. I-V curves are taken at 0.25, 0.5, and 1 sun illumination using a Spire 4600 SLP flash tester. EL and PL images are captured with a ZWO ASI183MM Pro 20.18 MP CMOS Monochrome Astronomy Camera. EL is conducted at 100% I_{SC}, and PL is conducted at approximately 1 sun illumination at 520 nm.

C. Data Processing & Analysis

I-V curve features are used to characterize electrical performance in a PV module, and were extracted from the raw I-V curves using the $ddiv$ package in R [19], [20]. These features include maximum power (P_{MP}), short circuit current (I_{SC}), open circuit voltage (V_{OC}), shunt resistance (R_{SH}), which measures leakage current loss, and fill factor (FF).

Multi-irradiance I-V curves were used to obtain an accurate series resistance (R_S) according to IEC 60891.

To analyze cracks in EL images of the mini-modules, we first reduce image noise by subtracting the corresponding dark frame from each biased EL and PL photo. Then, we extract each individual cell in the EL and PL images using the Harris Corner detector from the OpenCV Python module within our pvimage package in PyPI [21]. Each cell-level EL image is then standardized to be 1460 by 1460 pixels. Once images of the cells are extracted and standardized, we extract quantitative information about crack properties. Our previous studies have used supervised or unsupervised machine learning techniques to identify the presence of cracks [22]–[26]. Here we employ more traditional image processing methods to quantify crack features [27], [28]. To do this, we must apply several smoothing and coloring filters to obtain crack information. As

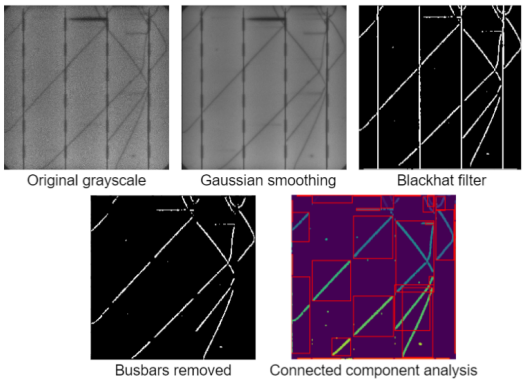

Fig. 1. Steps in digital image processing for crack detection.

seen in Figure 1, the images are originally in grayscale. We apply a Gaussian blur to reduce image noise. Then, we apply a blackhat filter and skeletonize the image to create a binary map of the cell cracks. The busbars in each image are removed by finding peaks in intensity along the x-axis and masking those regions in the binary maps. With the busbars removed, individual cracks are identified through connected component analysis.

The specific crack features we measure are: perimeter, area, convex area (area of the smallest encompassing convex polygon), and angle (measured with a linear fit and relative to the busbars). We also define a dendritic ratio, which quantifies the degree of branching in a cell crack, and is calculated by dividing the area of the crack by its convex area. The closer the dendritic ratio is to 0, the more branching the crack. Once all the crack features are collected, they are placed into a database for further analysis.

III. Results and Discussion

The results are grouped by cell type: Al-BSF or PERC. PERC modules experienced slightly more cracking, averaging 5.34 cracks per cell versus 4.60 cracks per Al-BSF cell. Because of the uncontrolled manner by which the modules were cracked, we cannot conclude whether one cell type is really more likely to crack. However, the large population of cell cracks allows us to study the statistical differences between the resulting crack properties and their effects on electrical performance for the two cell types.

The modules exhibited a wide range of electrical properties on both the cell and mini-module levels. In Figure 2, we see the EL images of four different modules, with varying degrees of cracking, from minimal to severe. Visually, we see that even though there are many severe cracks in both modules B and C, all cells in the PERC module (C) are relatively bright, while the Al-BSF module (B) has a darkened cell despite having fewer cracks.

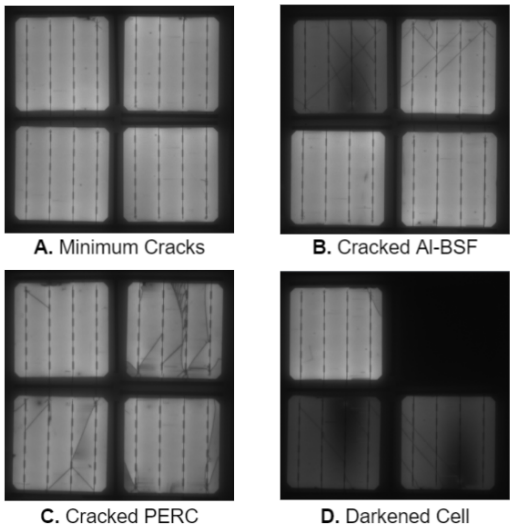

Fig. 2. Module visual comparison

The 1-sun I-V curves corresponding to the modules in Figure 2 are shown in Figure 3. There is significant shunting in module D, as shown by the dark cells in Figure 2, and all cracked modules (B-D) show greater R_S than the minimally cracked module A.

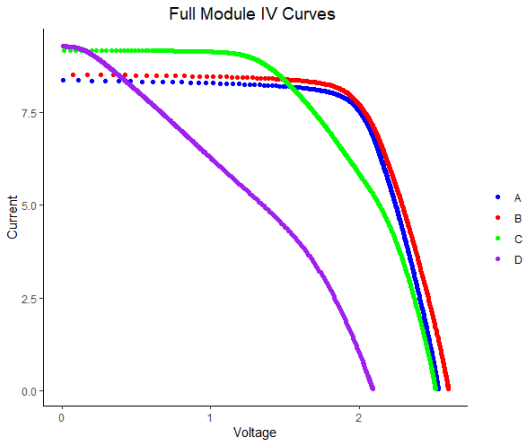

Fig. 3. Comparison of module-level I-V curves for modules shown in Figure 2.

The crack-related shunting behavior is confirmed by Figure 4 comparing EL and PL images of a severely damaged Al-BSF module. Darkened cells in EL images can result from high series resistance, shunts, or electrical isolation of cells or cell strings. Our mini-modules do not include bypass diodes between cells, so electrical isolation of even one cell would result in all cells being darkened. Series resistance effects that darken EL images do not affect PL measurements (as they do not require electrical contact). Therefore we conclude that the 3 cells that are completely dark in PL are shunted as a result of their cracks. (This cell darkening effect is well known from EL and PL image detection of PID, which also causes cell shunts.)

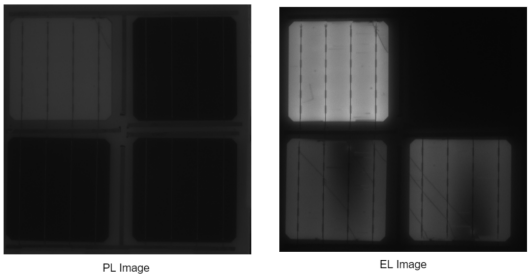

Fig. 4. PL and EL images of a cracked Al-BSF module.
insert correct module type.

In total, there were 8 Al-BSF modules with one or more cells that were too severely shunted to detect cracks in EL images. No PERC modules showed crack-related shunting to this degree. The median P_{MP} value for shunted Al-BSF cells was 0.720 W, and the median P_{MP} for an Al-BSF module with 1 or more shunted cells was 10.79 W. For non-shunted Al-BSF, the median P_{MP} values for cells and modules were 2.72 W and 14.86 W, respectively, demonstrating that cracking-related shunts in Al-BSF cells severely decreased their power production. Because it was not possible to extract crack properties from EL or PL images of the shunted cells, we omitted these cells and modules from further analysis.

A. *I-V Properties Distributions and Statistical Analysis*

Figure 5 shows the distribution of I_{SC}, V_{OC}, R_S, and P_{MP} on the cell level, while Figure 6 displays the distributions for module-level measurements. As expected, PERC modules had greater median values for each of the electrical properties shown, due to their inherent performance advantages and higher power conversion efficiency. Series resistance is likely higher for PERC due to their greater photocurrent.

Because we have no pristine (uncracked) samples, it is not possible for us to normalize the electrical properties for direct comparison of the two cell types. However, we can still qualitatively compare the differences in distributions of I-V properties for the different cell types, as well as correlations of I-V and crack characteristics. On both the cell and full module levels, Al-BSF modules showed greater variance in I-V properties than PERC modules. Variance of PERC I-V features was similar between the cell and module levels, while variance of Al-BSF I-V features was greater for module-level distributions. Because the two cell types were manufactured at the same facility using similar materials, we expect that the increased variance of Al-BSF I-V features is due to effects of cell cracks, and that this cell type may be more likely to experience electrical effects of cell cracking.

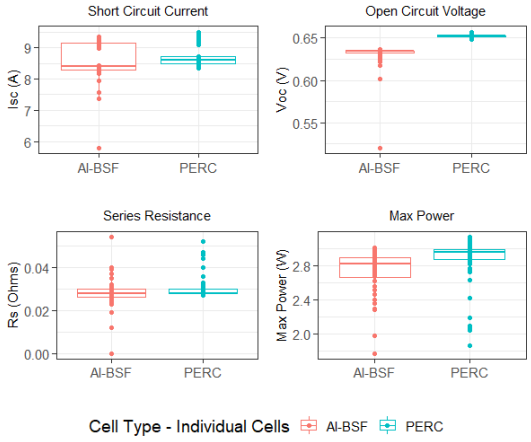

Fig. 5. Box plots of cell-level I-V feature distributions.

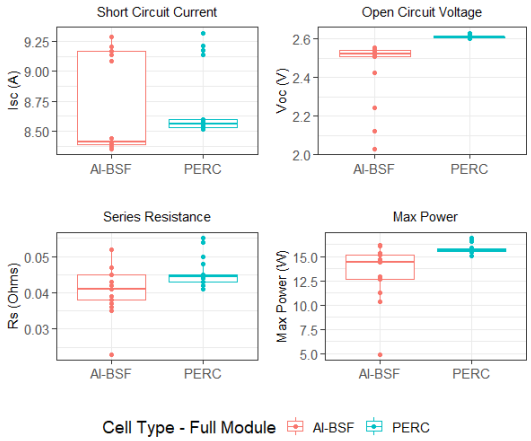

Fig. 6. Box plots of module-level I-V feature distributions.

B. *Crack Properties Distributions and Statistical Analysis*

Several crack properties were measured for analysis as described above. Figure 7 demonstrates the relationship between area and angle of detected cracks for both cell types. While there is obvious scatter in the data, larger area (longer) cracks only occur at small angles (parallel to busbars). This is due to the process of crack detection, which involves removing busbars from the image mask. This busbar removal artificially segments cracks that traverse the busbars into multiple segments, so the detected length of high angle cracks is limited by the distance between busbars at that angle.

Crack properties were statistically compared between the two module types. Here we present the data based on all individual cracks collected, cracks on the individual cell level,

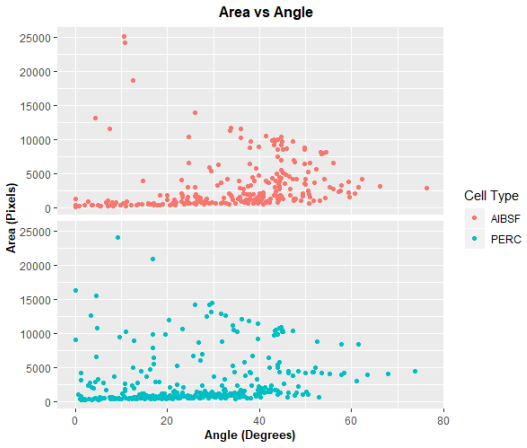

Fig. 7. Crack Area vs. Angle

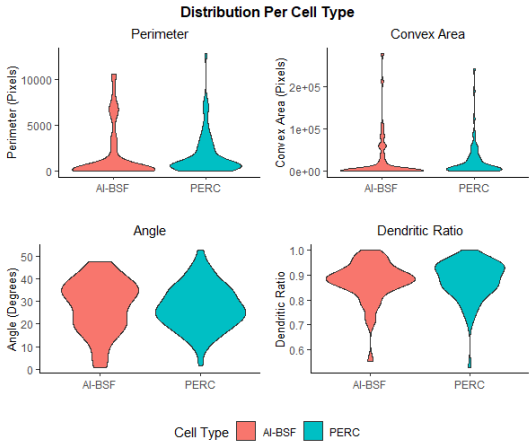

Fig. 9. Crack Properties on Cell Level

and cracks on the full module level. The first set of data visualized in Figure 8 shows crack distributions of all the cracks characterized in both Al-BSF and PERC modules. The violin plots show that the distributions for perimeter and convex area were both bottom heavy, indicating cracks tended to be short on both types of modules. The distributions on both types of cells were also top heavy for the dendritic ratio (area/convex area), suggesting that most cracks did not branch. As seen in the distribution plots for crack angle, cracks in PERC cells formed at a steeper angle (more parallel to busbars) than cracks in Al-BSF modules, which clustered around 45 degrees as expected for monocrystalline silicon cells.

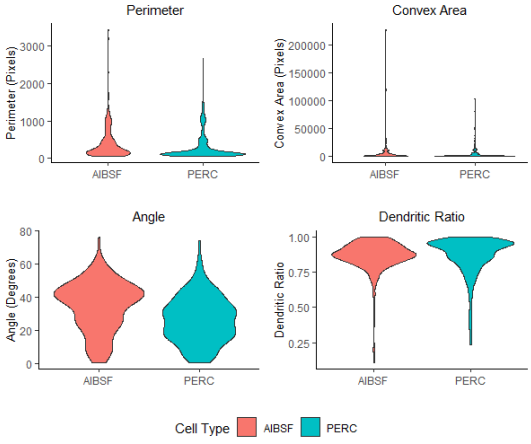

Fig. 8. Properties of All Detected Cracks

Figure 9 shows the distributions of crack properties as measured on the cell level. Perimeter and area measurements were summed over all cracks in each cell, and the dentritic ratio and angle were averaged. The cell-level distributions were similar to those for individual cracks, showing that the demonstrated crack properties are relatively consistent and can be compared with electrical properties at the cell level.

To study the distributions of crack properties on the full module level, areas were summed for all detected cracks in each module, and dendritic ratio and angle were averaged, as for the cell level measurements. The distributions of crack properties on the full module level as shown in Figure 10 were mostly similarly shaped than those for individual cracks or cell-level parameters. Modules still showed more smaller cracks than larger cracks, and had similar angle medians as on the cell level.

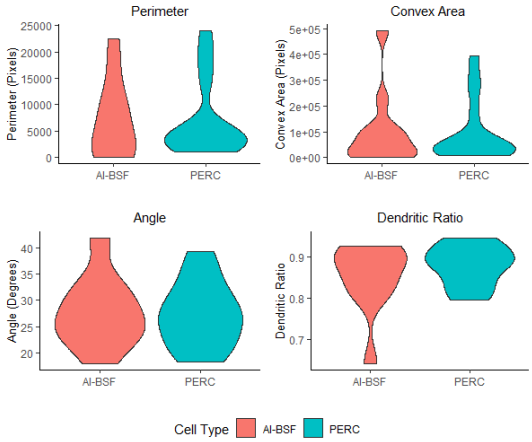

Fig. 10. Crack Properties on Full Module Level

We performed a Welch's T-Test at the 95% confidence interval to see if differences between cracking properties of Al-BSF and PERC were significantly different at the cell or module levels. These results are shown in Table I and II, respectively.

On the cell level, we see that there is no significant difference in crack properties between Al-BSF and PERC. This is also true for the module level measurements - crack properties were statistically similar between the two cell types.

C. Electrical and Crack Properties Correlation

Correlation plots were made to demonstrate the relationships between electrical properties and crack properties on

TABLE I
STATISTICAL ANALYSIS OF DIFFERENCES IN CRACK PROPERTIES ON THE CELL LEVEL.

	Al-BSF Median	PERC Median	p-value
Perimeter(Pixels)	1808	1812	0.994
ConvexArea(Pixels)	23800	24400	0.947
Angle(Degrees)	28.1	27.5	0.782
DendriticRatio	0.874	0.878	0.772

TABLE II
STATISTICAL ANALYSIS OF DIFFERENCES IN CRACK PROPERTIES ON THE MODULE LEVEL.

	Al-BSF Median	PERC Median	p-value
Perimeter(Pixels)	7240	7280	0.988
ConvexArea(Pixels)	102000	98500	0.954
Angle(Degrees)	27.8	27.4	0.899
DendriticRatio	0.852	0.878	0.386

both the individual cell and full module levels for both Al-BSF and PERC modules. Four plots were made: one for Al-BSF modules on the cell level, one for PERC modules on the cell level, one for Al-BSF modules on the full module level, and one for PERC modules on the full module level. These are shown in Figures 11, 12, 13, and 14, respectively.

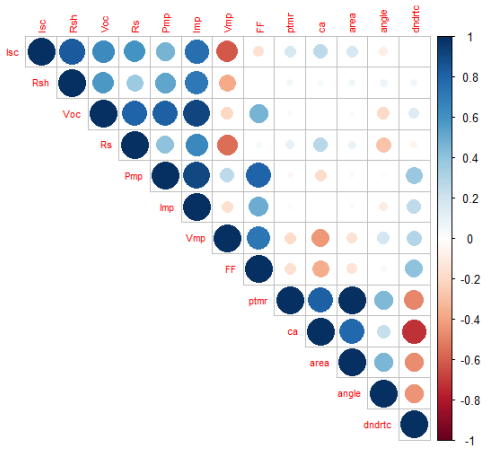

Fig. 11. Correlation plot for Al-BSF on the cell level

On the cell level, correlations between electrical and crack features were relatively weak. The strongest correlations between I-V and crack properties for Al-BSF cells were: P_{MP} and FF positively correlated with the average dendritic ratio (cells with more dendritic cracks had lower power); and V_{MP} negatively correlated with crack convex area (larger cracks cause higher R_S and lower V_{MP}). Crack and electrical properties of PERC cells tended to be more consistently correlated, but demonstrated different power loss mechanisms than Al-BSF. Cracks in PERC cells did not cause the R_S increase seen for Al-BSF, but do result in electrical isolation and mild shunting (I_{SC} and R_{SH} negatively correlated with crack length and area).

On the module level, correlations between crack and electrical properties are more prominent. Al-BSF modules show

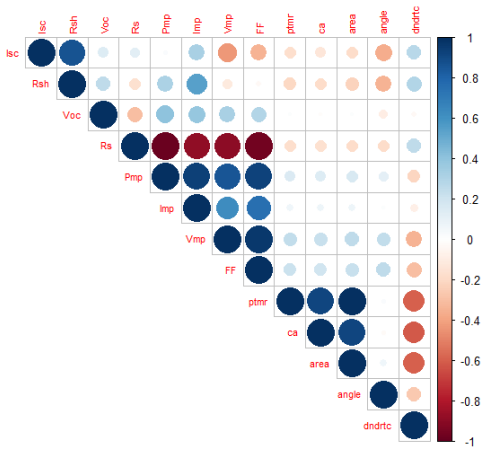

Fig. 12. Correlation plot for PERC on the cell level

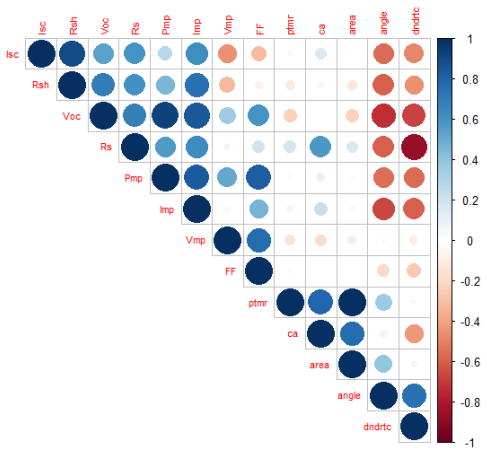

Fig. 13. Correlation plot for Al-BSF on the full module level

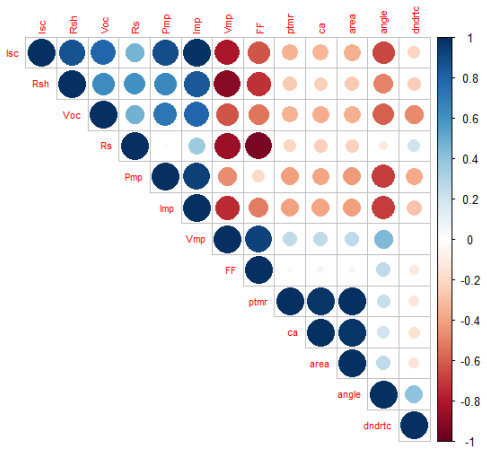

Fig. 14. Correlation plot for PERC on the full module level

strong negative correlations between several I-V features and crack angle and dendritic ratio. Specifically, linear cracks and cracks perpendicular to the busbars in Al-BSF modules are associated with greater power loss, shunting, current loss (electrical isolation), and recombination (lower V_{OC}). Meanwhile, cracks that are dendritic, more parallel to the busbars, or of large convex area are associated with series resistance increases in Al-BSF modules.

PERC modules did not demonstrate the strong relationships between I-V features and dendritic ratio that occurred for Al-BSF. However, these modules did show negative correlations between all other crack properties and nearly all electrical features. Larger cracks caused greater power loss in PERC modules, associated with decreases in I_{SC}, V_{OC}, and R_{SH}. Crack angle was also important in PERC modules, with cracks perpendicular to the busbars again causing greater power loss as for Al-BSF.

IV. Conclusions

In this work, we demonstrated an automated process for identifying and quantitatively characterizing PV cell cracks in EL images, and statistically comparing the resulting crack properties to electrical performance of modules. We used this process to compare crack properties and effects on electrical performance in PERC and Al-BSF mini-modules that experienced transportation-related cell cracking. Several Al-BSF modules experienced severe shunting and power loss associated with cell cracks. Cell shunts resulting from cell cracks have not been previously demonstrated in the literature. In addition to greater susceptibility to crack-related shunts, cracked Al-BSF modules that did not suffer catastrophic power loss showed greater variance in electrical properties than cracked PERC modules, despite no statistically significant difference between the types and severity of cracks for these two cell types. Correlation plots for electrical and crack properties of Al-BSF and PERC cells and modules demonstrated different crack-related power loss mechanisms for the two cell types. Power loss in PERC modules was associated with more total crack length, resulting in electrical isolation of cell areas and mild shunting and recombination. Power loss in Al-BSF modules was not as strongly correlated with total crack length; instead the crack angles and branching were better indicators of module performance for this cell type. This work suggests that Al-BSF modules are more likely than PERC modules to suffer power loss as a result of cell cracking, despite the two cell types being similarly susceptible to cracking.

References

[1] M. Köntges, M. Siebert, A. Morlier, R. Illing, N. Bessing, and F. Wegert, "Impact of transportation on silicon wafer-based photovoltaic modules: Impact of transportation on photovoltaic modules," *Progress in Photovoltaics: Research and Applications*, vol. 24, no. 8, pp. 1085–1095, Aug. 2016. [Online]. Available: http://doi.wiley.com/10.1002/pip.2768

[2] K. Strohkendl, W. Herrmann, W. Vaassen, J. Althaus, and F. Reil, "The Effect of Transportation Impacts and Dynamic Load Tests on the Mechanical and Electrical Behaviour of Crystalline PV Modules," *25th European Photovoltaic Solar Energy Conference and Exhibition / 5th World Conference on Photovoltaic Energy Conversion, 6-10 September 2010, Valencia, Spain*, pp. 3989–3992, Oct. 2010. [Online]. Available: http://www.eupvsec-proceedings.com/proceedings?paper=6678

[3] V. Gupta, M. Sharma, R. Pachauri, and K. N. D. Babu, "Impact of hailstorm on the performance of PV module: a review," *Energy Sources, Part A: Recovery, Utilization, and Environmental Effects*, vol. 0, no. 0, pp. 1–22, Aug. 2019. [Online]. Available: https://doi.org/10.1080/15567036.2019.1648597

[4] M. Köntges, S. Kurtz, C. E. Packard, U. Jahn, K. A. Berger, K. Kato, T. Friesen, H. Liu, M. Van Iseghem, J. Wohlgemuth, D. Miller, M. Kempe, P. Hacke, F. Reil, N. Bogdanski, W. Herrmann, C. Buerhop-Lutz, G. Razongles, and G. Friesen, "Review of Failures of Photovoltaic Modules," IEA International Energy Agency, Report, 2014. [Online]. Available: https://repository.supsi.ch/9645/

[5] C. Buerhop, S. Wirsching, A. Bemm, T. Pickel, P. Hohmann, M. Nieß, C. Vodermayer, A. Huber, B. Glück, J. Mergheim, C. Camus, J. Hauch, and C. J. Brabec, "Evolution of cell cracks in PV-modules under field and laboratory conditions," *Progress in Photovoltaics: Research and Applications*, vol. 26, no. 4, pp. 261–272, 2018. [Online]. Available: https://onlinelibrary.wiley.com/doi/abs/10.1002/pip.2975

[6] M. Köntges, I. Kunze, S. Kajari-Schröder, X. Breitenmoser, and B. Bjørneklett, "The risk of power loss in crystalline silicon based photovoltaic modules due to micro-cracks," *Solar Energy Materials and Solar Cells*, vol. 95, no. 4, pp. 1131–1137, Apr. 2011. [Online]. Available: http://www.sciencedirect.com/science/article/pii/S0927024810007129

[7] N. Bosco, J.-N. Jaubert, L. Mao, J. Liu, J. Carter, and R. French, "Employing Fracture Statistics to Track Cell Reliability Through Module Fabrication," in *2020 47th IEEE Photovoltaic Specialists Conference (PVSC)*, Jun. 2020, pp. 0263–0265.

[8] M. Dhimish, V. Holmes, M. Dales, and B. Mehrdadi, "Effect of micro cracks on photovoltaic output power: case study based on real time long term data measurements," *Micro & Nano Letters*, vol. 12, no. 10, pp. 803–807, Oct. 2017. [Online]. Available: https://digital-library.theiet.org/content/journals/10.1049/mnl.2017.0205

[9] M. Sander, S. Dietrich *et al.*, "Influence of manufacturing processes and subsequent weathering on cell cracks in pv modules," in *28th EU PVSEC*, 2013. [Online]. Available: http://www.eupvsec-proceedings.com/proceedings?paper=25164

[10] E. J. Schneller, H. Seigneur, J. Lincoln, and A. M. Gabor, "The impact of cold temperature exposure in mechanical durability testing of pv modules," in *2019 IEEE 46th Photovoltaic Specialists Conference (PVSC)*. IEEE, 2019, pp. 1521–1524.

[11] C. A. R. Castañeda, S. Chattopadhyay, J. Oh, S. Tatapudi, G. Tamizh-Mani, and H. Hu, "Field Inspection of PV Modules: Quantitative Determination of Performance Loss due to Cell Cracks Using EL Images," in *2017 IEEE 44th Photovoltaic Specialist Conference (PVSC)*, Jun. 2017, pp. 1858–1862.

[12] A. Danilewsky, J. Wittge, K. Kiefl, D. Allen, P. McNally, J. Garagorri, M. R. Elizalde, T. Baumbach, and B. K. Tanner, "Crack propagation and fracture in silicon wafers under thermal stress," *Journal of Applied Crystallography*, vol. 46, no. 4, pp. 849–855, Aug. 2013. [Online]. Available: http://scripts.iucr.org/cgi-bin/paper?S0021889813003695

[13] A. Morlier, F. Haase, and M. Köntges, "Impact of Cracks in Multicrystalline Silicon Solar Cells on PV Module Power—A Simulation Study Based on Field Data," *IEEE Journal of Photovoltaics*, vol. 5, no. 6, pp. 1735–1741, Nov. 2015.

[14] M. Sander, S. Dietrich, M. Pander, M. Ebert, S. Thormann, J. Wendt *et al.*, "Investigations on cracks in embedded solar cells after thermal and mechanical loading," in *27th European Photovoltaic Solar Energy Conference and Exhibition*, 2012, pp. 3188–3193.

[15] T. Trupke, B. Mitchell, J. W. Weber, W. McMillan, R. A. Bardos, and R. Kroeze, "Photoluminescence Imaging for Photovoltaic Applications," *Energy Procedia*, vol. 15, no. Supplement C, pp. 135–146, Jan. 2012. [Online]. Available: http://www.sciencedirect.com/science/article/pii/S1876610212003529

[16] S. Spataru, P. Hacke, D. Sera, S. Glick, T. Kerekes, and R. Teodorescu, "Quantifying solar cell cracks in photovoltaic modules by electroluminescence imaging," in *2015 IEEE 42nd Photovoltaic Specialist Conference (PVSC)*, Jun. 2015, pp. 1–6.

[17] M. Köntges, S. Kajari-Schröder, I. Kunze, and U. Jahn, "Crack statistic of crystalline silicon photovoltaic modules," in *26th European Photovoltaic Solar Energy Conference and Exhibition*, 2011, pp. 5–6. [Online]. Available: http://isfh.de/institut_solarforschung/files/26eupvsec_koentges.pdf

[18] S. Kajari-Schröder, I. Kunze, and M. Köntges, "Criticality of Cracks in PV Modules," *Energy Procedia*, vol. 27, no. Supplement C, pp. 658–663, Jan. 2012. [Online]. Available: http://www.sciencedirect.com/science/article/pii/S1876610212013380

[19] X. Ma, W.-H. Huang, E. Schnabel, M. Köhl, J. Brynjarsdóttir, J. L. Braid, and R. H. French, "Data-driven i–v feature extraction for photovoltaic modules," *IEEE Journal of Photovoltaics*, vol. 9, no. 5, pp. 1405–1412, 2019.

[20] Wei-Heng Huang, Xuan Ma, Jiqi Liu, Menghong Wang, Alan J. Curran, Justin S. Fada, Jean-Nicolas Jaubert, Jing Sun, Jennifer L. Braid, Jenny Brynjarsdottir, Megan M. Morbitzer, Roger H. French, and Roger H. French, "ddiv: Data Driven I-V Feature Extraction," Apr. 2021. [Online]. Available: https://CRAN.R-project.org/package=ddiv

[21] A. M. Karimi, B. G. Pierce, J. S. Fada, N. A. Parrilla, R. H. French, and J. L. Braid, "PVimage: Package for PV Image Analysis and Machine Learning Modeling," May 2020. [Online]. Available: https://pypi.org/project/pvimage/

[22] J. S. Fada, M. A. Hossain, J. L. Braid, S. Yang, T. J. Peshek, and R. H. French, "Electroluminescent Image Processing and Cell Degradation Type Classification via Computer Vision and Statistical Learning Methodologies," in *2017 IEEE 44th Photovoltaic Specialist Conference (PVSC)*, Jun. 2017, pp. 3456–3461.

[23] A. M. Karimi, J. S. Fada, J. Liu, J. L. Braid, M. Koyutürk, and R. H. French, "Feature Extraction, Supervised and Unsupervised Machine Learning Classification of PV Cell Electroluminescence Images," in *2018 IEEE 7th World Conference on Photovoltaic Energy Conversion (WCPEC) (A Joint Conference of 45th IEEE PVSC, 28th PVSEC 34th EU PVSEC)*, Jun. 2018, pp. 0418–0424. [Online]. Available: https://ieeexplore.ieee.org/abstract/document/8547739

[24] A. M. Karimi, J. S. Fada, M. A. Hossain, S. Yang, T. J. Peshek, J. L. Braid, and R. H. French, "Automated Pipeline for Photovoltaic Module Electroluminescence Image Processing and Degradation Feature Classification," *IEEE Journal of Photovoltaics*, vol. 9, no. 5, pp. 1324–1335, Sep. 2019.

[25] A. M. Karimi, J. S. Fada, N. A. Parrilla, B. G. Pierce, M. Koyuturk, R. H. French, and J. L. Braid, "Generalized and Mechanistic PV Module Performance Prediction From Computer Vision and Machine Learning on Electroluminescence Images," *IEEE Journal of Photovoltaics*, vol. 10, no. 3, pp. 878–887, May 2020. [Online]. Available: https://ieeexplore.ieee.org/document/9050914/

[26] Benjamin G. Pierce, Ahmad Maroof Karimi, JiQi Liu, Jennifer L. Braid, and Roger H. French, "Identifying Degradation Modes of Photovoltaic Modules Using Unsupervised Machine Learning on Electroluminescense Images," in *PVSC 47*. Virtual: IEEE, Jun. 2020. [Online]. Available: https://www.ieee-pvsc.org/virtual/index.php?page=presentation&session_id=53&presentation_id=291

[27] C. M. Whitaker, B. G. Pierce, A. M. Karimi, R. H. French, and J. L. Braid, "PV Cell Cracks and Impacts on Electrical Performance," in *2020 47th IEEE Photovoltaic Specialists Conference (PVSC)*, Jun. 2020, pp. 1417–1422.

[28] Jennifer L. Braid, Joshua S. Stein, Benjamin G. Pierce, Nicholas A. Parrilla, Ahmad Maroof Karimi, and Roger H. French, "Quantifying Cell Fractures in Si PV Modules," Lakewood, Colorado, Feb. 2020. [Online]. Available: https://pvrw.nrel.gov/program